Investigation of Magnetic Nozzle Plasma Detachment Using Scaled Down Pulsed Micro-Thruster

IEPC 2013-431

Presented at the 33rd International Electric Propulsion Conference,
The George Washington University • Washington, D.C. • USA
October 6 – 10, 2013

T.E.R. Smith[1], T. Zhuang[2], M. Keidar[3]
George Washington University, Washington, DC, 20052

Abstract: A design for an experiment demonstrating the resistive method of plasma detachment is explored for use on the Micro-Cathode Arc Thruster (μCAT) at the George Washington University (GWU). This resistive method involves the creation of an induced magnetic field traveling in the toroidal direction of the initial plasma flow, which is traveling in the poloidal direction. These fields are achieved by adding an outer annulus ring to the magnetic nozzle. The results from the experiments on the μCAT pulsed plasma thruster could be scaled upwards for use in full-sized pulsed power spacecraft, such as Magneto-Inertial Fusion (MIF) plasma. In the concluding remarks, two mathematical challenges are mentioned: firstly, the collimation experiments simulating solar phenomenon utilized a continuous plasma source, whereas for the proposed case, the plasma source will be pulsed, and secondly, the size must be scaled upwards from the laboratory scale to the fusion spacecraft scale.

Nomenclature

a Flux Tube Radius
A Area
B Magnetic Field
c_s Sound Speed
dN/dt Number of Reactivities per Second
γ Growth Rate of Instability
e Electric Charge
E Electric Field
g Gravity
I Current
I_{sp} Specific Impulse
j Current
K Magnetic Helicity
L Column Length
m Electron Mass
M Ion Mass
M (also refers to Spacecraft Mass)
$\dot{M}$, dM/dt Mass Flow Rate

[1] PhD Candidate, tsmith25@gwmail.gwu.edu
[2] PhD Graduate of GWU, zhuangts@gwu.edu
[3] Professor, keidar@gwu.edu

μ Magnetic Permeability
ω Frequency
P Pressure
ρ Density
S Lundquist Number
σv Plasma Reactivity
T Temperature
Th Thrust
t Time
τ_A Alfven Time Scale
V Velocity
Ψ Poloidal Magnetic Flux
r, Θ, z Radial, Polodial, and Axial (along the nozzle) Directions
x, y, z Flow, Shear Flow, and Outgoing Flow in the Axial Direction

I. Introduction

Research conducted in the field of plasma engineering and magnetic nozzles for fusion and other advanced spacecraft have been developing more sophisticated methods for enhancing plasma flow. This research explores the possibility for using the resistive method of plasma detachment for magnetic nozzles. Experiments that have been conducted previously for laboratory-sized plasma collimation are adapted for implementation onto the μCAT device at GWU. These prior experiments, in which Kelvin Helmholtz (KH) instability and flux tubes were purposefully created, were done in order to better understand plasma outflows from stellar objects, such as young black holes and active galactic nuclei. Resistive detachment has been demonstrated experimentally [1] for the simulation of the detachment of plasma from the Sun, in which a voltage bias between an inner disk electrode and outer annulus electrode replaced the function of rotating mass of plasma on the surface of the Sun, since the shear plasma flow is what is responsible for generating an accumulation of plasma along the toroidal direction, and detachment along the axial direction. The addition of an outer annulus is proposed, to fit around the outside of the magnetic coil nozzle of the GWU thruster with the micro-cathode arc generated plasma on the inside of the thruster as the inner source, rather than an inner disk with gas feed.

II. Detachment Mechanisms

Detachment is an issue that affects multiple types of spacecraft that utilize magnetic nozzles, such as fusion spacecraft, fission fragment spacecraft, and other spacecraft that eject plasma. Meridional magnetic nozzle concept studies have been conducted using MHD code to study this magnetic field and various conditions for nozzle flow and wall loading from plasma processes, and transport and radiation losses were studied for cold plasmas and warm plasmas, ranging from 1 eV to 100 eV [2]. Warm plasmas are considered to be collisionless plasmas, and can undergo instabilities, such as the Rayleigh-Taylor instability in the nozzle throat [2]. The Kelvin Helmholtz instability is also present due to the sheared E x B drift velocity.

The variations in the plasma also can determine how that plasma is able to detach itself from the magnetic field of the nozzle. For instance, in order for dense plasma to escape, the ions and electrons stay together in order to maintain quasineutrality. As listed by Sankaran (2007) [3], there are several ways to address the detachment problem. Firstly, there is resistive detachment, secondly kinetic detachment, thirdly recombination detachment, fourthly non adiabatic detachment, and fifthly electron inertia detachment. The resistive method for plasma detachment is described as being driven by collisions in the plasma, or by the amount of resistivity experienced by the particles, as electrons may also face resistance upon undergoing anomalous transport from turbulent waves.

The VASIMR team [4] investigated the theoretical possibility of generating resistive, frozen-in flux as a method of detachment, which requires a reconnection event at super-Alfvenic speeds. This investigation assumed the cold plasma conditions of the VASIMR spacecraft. Cold plasma omits a pressure term from the MHD equations, and they also assumed steady state conditions. They state that a conical nozzle presents the unique feature of generating a sub to super Alfenic plasma flow transition without acceleration due to the decrease of the magnetic field downstream.

Analysis conducted by Polzin and Sankaran (2009) [5] states that the issue of detachment may be addressed when the kinetic energy (due to the high velocity) of the plasma coming out of the nozzle ($\frac{1}{2}mv^2$) is much greater than $\frac{1}{2}\mu B^2$. Furthermore, once plasma exits the nozzle, the magnetic field lines are stretched, such that B_2, B_3, … B_n going into space become weaker and weaker (such that, $B_n << B_1$), meaning that the plasma also gets faster the further away it gets from the nozzle [5].

Additional comparison studies have been made for magnetic nozzle plasma detachment, by means of the diffusive method caused by either plasma resistivity or electron-inertia [6], or magnetic stretching. In these studies, cold plasma is assumed for use in helicon thrusters [4], to explain how resistive detachment is preferable over other methods, which tend to fail due to problems such as field geometries or issues in plasma dynamics. The importance of magnetic detachment, in order to have plasma detachment, is discussed, and it is concluded that magnetic detachment is divergent for the diamagnetic Hall current dominant over the paramagnetic swirl current [7]

A. Kelvin Helmholtz and Velocity Sheer

Mathematical simulations assuming the influence of a Kelvin-Helmholtz Instability [8] have successfully generated the twisted flux tubes observed in an event of plasma collimation and detachment on the Sun. The mathematical simulations of the flux tubes, which are similar to solar helmet streamers and tails that come off the magnetic field of planets and plasmas of stars, assume the following mathematical processes:

Instabilities can lead to the creation of plasma flux tubes, which can be designed to stretch critically when reconfigured to release plasma. During this process, chaos (as a result of the nonlinear nature of the situation) will be occurring in these higher degrees of freedom with multiple waves. Specifically, the Kelvin-Helmholtz instability can generate twisted flux tubes, and Lapenta (2003, 2005) [8][11] "showed simulations in which instability [via the KH instability] compresses the magnetic field, leading to reconnection and the formation of islands or twisted flux tubes." It is important to understand instabilities such as these, in order to control and apply them (or negate their existence), once plasma is re-released.

Chaotic dynamics does not necessarily mean diffusion. Chaotic dynamics thrive in non-linear systems - especially for higher degrees of freedom, but diffusion only occurs for many "collisions" or in other words decorrelations between the particles and the driver(s). In this case, there is a warm beam of collisionless plasma, damped by the mechanism of Landau wave damping [12]. So far, there are two kinds of resonances that are addressed in this system: gyro motion and bouncing motion. Resonance with the gyro frequency cause diffusion across the field lines: the perpendicular energy increases so that the particles gyrate at larger radii away from the central field line (or vice versa).

On the Sun, shear Alfven waves introduce the presence of velocity shear $v_{shear,y}(x,z)$ in the plasma flow, with z being the direction of the outgoing plume and y the direction of the shear, which transmits photospheric motion to the plasma on the corona. The velocity shear can also be introduced by lower-hybrid drift instability, and kinetic simulations on current sheets have shown that the growth rate γ of KH instability increases linearly with added velocity shear

$$\gamma \sim k v_{shear,y}(x,z) \tag{1}$$

with k being the wave number. The growth rate of instability encourages field detachment and the generation of magnetic islands, bordered by seperatrices [8], and the magnetic field lines then reconnect on the other end of the seperatrices due to flux pileup. This was demonstrated computationally, studying current sheets using Harris magnetic field configurations and by studying the compression and rarefaction of the plasma in different locations, demonstrating that recombination of magnetic field lines in the compression regions occurred on the KHI time scale [8][9][10]. The velocity shear will drive the growth rate of instability, regardless of the resistivity of the plasma, in the same manner as the tearing instability, which is determined by the resistance faced in the plasma, according to:

$$\gamma \tau_A \sim S^{-\frac{3}{5}} \tag{2}$$

where τ_A is the Alfven time scale, which is approximately equal to L_B/v_A (the length scale of the variation of the magnetic field over the Alfven velocity), and S is the Lundquist number [8].

B. Collimation and Spheromak Formation

A plasma jet is formed from the shear velocity flow, which results in a poloidal velocity field and an induced toroidal magnetic field, as seen in Fig. 1. Prior computational simulations utilizing the mathematics of the KH Instability simulations agree with spheromak experiments [13] [14], which demonstrated toroidal twisted flux tube reconnection, in measuring quadrupolar configurations of out-of-field, collisionless MHD fields. The collimation method has been conducted [1] [15] to demonstrate similar phenomena at a laboratory scale. In the collimation method, a flux tube is created, designed to stretch critically when reconfigured to release plasma. A probe with a high sampling rate is used to pick up data about the resulting waves.

As it applies to solar plasma dynamics, this law **E** + **v** x **B** = 0 demonstrates that an electric field will be induced due to a sheared toroidal rotation of a disk of plasma on the surface of the Sun in the presence of a magnetic field, **B**. The Hsu experiment [1] was conducted by injecting a magnetic helicity K rather than simulating the rotating of a mass of plasma, and the magnetic helicity emanated outwards at a rate of $dK/dt = 2\psi V$, where ψ was the poloidal magnetic flux being emitting from the center, and V was the potential drop between the point at which r=0 on the center of the accreting disk of plasma.

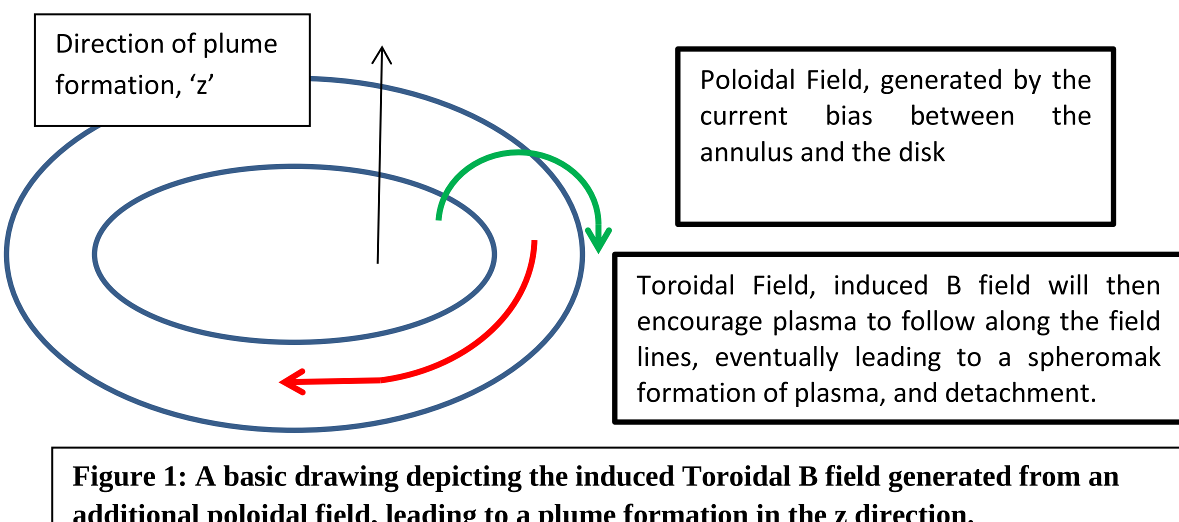

Figure 1: A basic drawing depicting the induced Toroidal B field generated from an additional poloidal field, leading to a plume formation in the z direction.

The plasma traveled along the magnetic field lines, which can be described as follows:

$$\nabla \times \boldsymbol{B} \cong \alpha_{gun}\boldsymbol{B} \tag{3}$$

with the B field being determined by a factor α_{gun}, an adjustable eigenvalue that was demonstrated experimentally, varying according to $\alpha_{gun} = \mu_0 I_{gun} / \psi_{gun}$ and dependent on varying the current I_{gun} and poloidal flux intercepting the inner disc electrode ψ_{gun} [1].

Plasma would gather in the center and collimate, and the collimated plasma would then lead to detachment for high values of α_{gun}, specifically for $\alpha_{gun} \sim 129\ m^{-1}$. The physical mechanism for detachment post-collimation is speculated to be due to plasma forming into a spheromak configuration. The presence of plasma in the spheromak formation has been experimentally verified, for the collimation method [15]. For the experiment, the outer foot points of the annulus are at a diameter of four to five times that the inner foot points [1]. As the legs fill up with plasma, they merge to form a single column. The central column eventually kinks to become a spheromak [1][15].

III. Plasma flow through a nozzle

Steady plasma flow through a magnetic nozzle, (*prior to* the addition of the outer annulus modification which would include shear motion at the exit), can be described using ideal, steady flow MHD equations. Beginning with these equations, assuming a meridional configuration in which $\mathbf{B} = (B_r, 0, B_z)$ due to axisymmetry $\boldsymbol{v}_\theta = \boldsymbol{B}_\theta = 0$,

$$\begin{gathered} \rho\boldsymbol{v} \cdot (\boldsymbol{v}\boldsymbol{\nabla}) = [\mathbf{J} \times \mathbf{B}] \\ \boldsymbol{v} \cdot \boldsymbol{\nabla}(P\rho^{-\gamma}) = 0 \\ \boldsymbol{\nabla} \cdot (\rho\boldsymbol{v}) = 0 \\ \boldsymbol{\nabla} \times [\boldsymbol{v} \times \boldsymbol{B}] = 0 \\ \boldsymbol{\nabla} \cdot \boldsymbol{B} = 0 \end{gathered} \tag{4}$$

The ratios for P Pressure, v velocity, ρ density, and T temperature can be found according to their relationship to the B field ratios.

$$\frac{B}{B_0} = \frac{v}{v_0}\left[\frac{4}{3} - \frac{1}{3}\left(\frac{v}{v_0}\right)^2\right]^{\frac{3}{2}} \tag{5}$$

The subscript 0 indicates the location at the throat, which is equation to the sound speed [2]. The sound speed equation $c_s = \left(\frac{\gamma P}{\rho}\right)^{\frac{1}{2}}$ can be used to demonstrate the relationship between the sound speed at the throat and the exhaust velocity, and for an assumed value of $\gamma = 5/3$ for Hydrogen it is:

$${c_{s0}}^2 = \frac{3}{4}c_{SR}^2 = \frac{1}{4}v_e^2 \tag{6}$$

The subscript R depicts the sound speed in the reservoir. Solving for v/v_0, using the quadratic formula

$$\frac{v}{v_0} = \left[\sqrt{y} \pm \sqrt{\sqrt{4y^2 - 3(\frac{B}{B_0})^{\frac{2}{3}}} - y}\right]^{\frac{3}{2}} \quad (7)$$

With + and – being super or subsonic flow, and with y being

$$y = \frac{1}{2}\left[\sqrt{1 + \sqrt{1 - \left(\frac{B}{B_0}\right)^2}} + \sqrt{1 - \sqrt{1 - \left(\frac{B}{B_0}\right)^2}}\right] \quad (8)$$

This demonstrates that an modification in the magnetic field at the exit of the nozzle, would lead to a modified magnetic field ratio with the magnetic field at the nozzle throat. The goal is to have an increase in the exit velocity, thus increasing the I_{sp} specific impulse and thrust of the spacecraft, according to

$$I_{sp} = \frac{v_e}{g} \quad (9)$$

$$Th = I_{sp} g \dot{M} \quad (10)$$

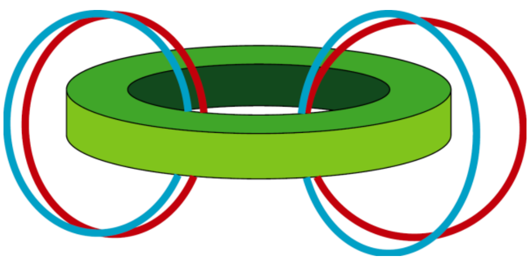

Figure 2.a. and Figure 2.b. [16] The field lines for the magnetic coil, seen from the side, for the µCAT to be modified, with 2.a. emphasizing that the plasma flow also follows the magnetic field lines in the poloidal direction. The cathode spot is pointed out in 2.b. The Cathode spots would be multiplied to occur in several places and aligned symmetrically with the outer annulus, which would have concurring spots.

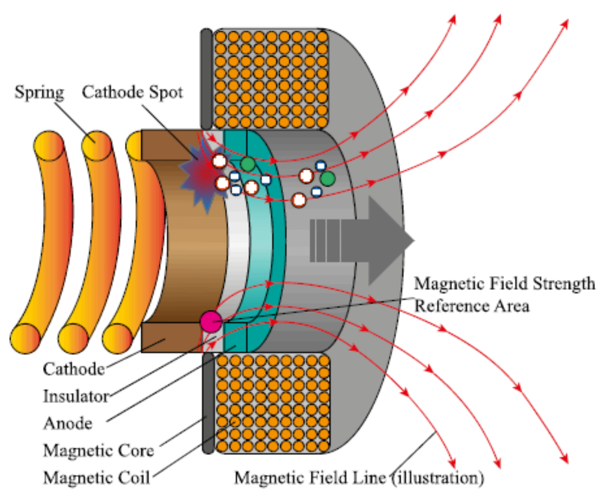

In calculating the potential specific impulse for a given exhaust velocity, the mass flow rate can be obtained from the thrust equation. Additionally, for the quasi-1D approximation: $\frac{dM}{dt} \sim \rho_0 v_0 A$, which shows the possibility of obtaining a theoretical throat velocity and area, and from the modified thrust equation,

$$Th = \frac{5}{3}(A_0 P_R) \quad (11)$$

Where the pressure of the reservoir P_R can be assumed for a theoretical magnetic nozzle thrust, for the calculated mass flow rate. The nozzle of the thruster has an initial **B** field that loops around the magnetic coil of the µCAT poloidally. The field lines for the outgoing plasma follow the magnetic field lines, as depicted in Fig. 2.a. and Fig. 2.b.

A. Adding the Outer Annulus

Assuming steady state for $E_\theta = 0$, the meridional velocity is lined up with the magnetic field, such that $\mathbf{v_M} = \alpha \mathbf{B_M}$. Originally, the equation $dK/dt = 2\psi V$ demonstrated how the applied voltage bias between the outer electrodes would generate a magnetic field (induced) toroidally. Now the voltage we will assume is the voltage applied to the thruster in order to generate outgoing plasma, at least initially. The goal is to generate spider legs of plasma which will conjoin with an outer annulus ring, in order to study the creation of flux tubes using KH instability, and the potential for detachment from the magnetic coil. The Hsu study utilized an external solenoid to produce poloidal bias magnetic flux to link the inner electrodes (receiving negative polarity high voltage) and outer electrodes (ground) and gas lines to deliver the fast puffs of neutral gas to breakdown adjacent to the electrodes. Gas feed may be necessary for the outer electrode annulus for the GWU thruster, which would fit along the outer rim of the magnetic coil. The magnetic coil would provide the magnetic flux.

The current of the plasma would not be sufficient for one spark of plasma generated by the micro-thruster, and so there would need to be several distinct locations for generating plasma simultaneously in order to generate the sufficient current needed, for the plasma to meet between the inner disk and outer annulus, and to form a collimating and detaching plasma structure. The proposed parts to be manufactured for augmenting the thrust as it comes out of the nozzle and encouraging collimation can be seen in Fig 3.

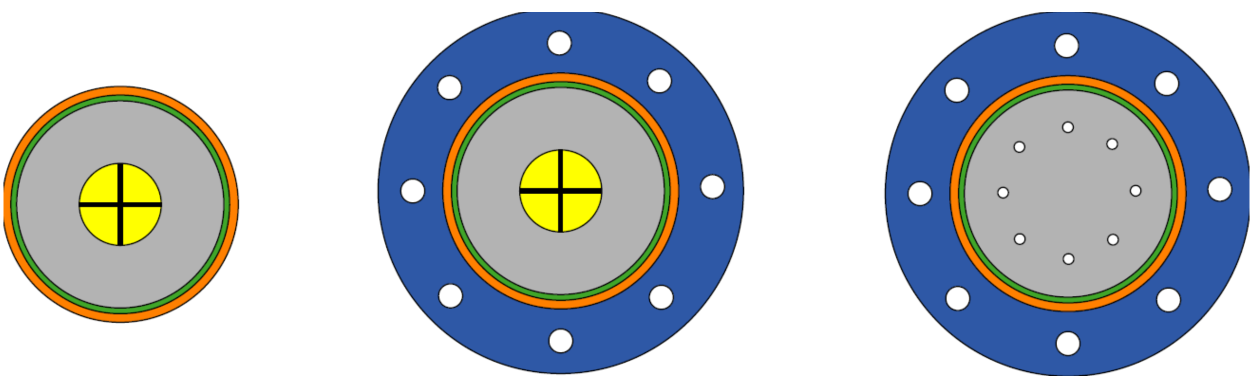

Figure 3 Proposed configuration of outer electrode ring, situated on the outside of the magnetic coil (the nozzle). Instead of an inner disk as was utilized in the Hsu experiment, the plasma could instead be generated on specific points on the cathode. Furthermore, the points of plasma generation on the cathode could be more or less than 8 points, as long as symmetry is maintained with the outer annulus.

For the experiments conducted on µCAT, the inductor current reached about 38 Amps of current at the moment discharge between the electrodes, which underwent an input voltage of 22V, while the discharge voltage of 50 V remains constant throughout the process. The Hsu experiment applies a voltage of 4-6 V across the gap in order to drive a current of 70-130 kA for the plasma to travel along. The plasma would then propagate outward in the form as a helical plume, at a velocity of 6 x 10^6 m/s. The initial parameters for μCAT demonstrated a plasma velocity at 19 x 10^3 m/s for a magnetic field of 0 T and a plasma velocity of 31 x 10^3 m/s for a magnetic field of 0.3 T [16]. The exit velocity for the thruster was calculated for μCAT using the following equations which utilized radial and poloidal currents:

$$Mn\frac{dV}{dt} = j_\theta B_r \tag{12}$$

$$j_\theta = \left(\frac{\omega_e}{v_{ei}}\right) j_r \tag{13}$$

$$j_{er} = j_{ir} = enV_r \tag{14}$$

ω_e is the electron cyclotron frequency, j_θ is the azimuthal electron current, v_{ei} is the electron ion collision frequency, and j_r is the current in the radial direction. The ion velocity in the axial direction is thus

$$\Delta v_z \approx \sqrt{\frac{2e^2 B_z B_r V_r \Delta z}{mMv_{ei}}} \tag{15}$$

With the addition of the outer annulus outside of the magnetic coil, and thus the addition of the radial current, a greater discharge velocity may be achieved, since a higher current to density ratio is shown to give a greater exhaust velocity in the z direction. Furthermore, according to Ohm's Law I = V/R, a higher current indicates a comparatively higher voltage to resistance ratio. The greater number of spider legs may require a greater input of current, and the voltage would be calculated for a circuit to include each leg. Future experiments will explore what geometrical configuration would be best, for the generated circuits. The geometrical growth is explained simply for the development of a detaching helical plasma structure from an accretion of plasma in the center. A drawing for the modified lines of current along the applied and induced B fields are shown in Fig. 4.

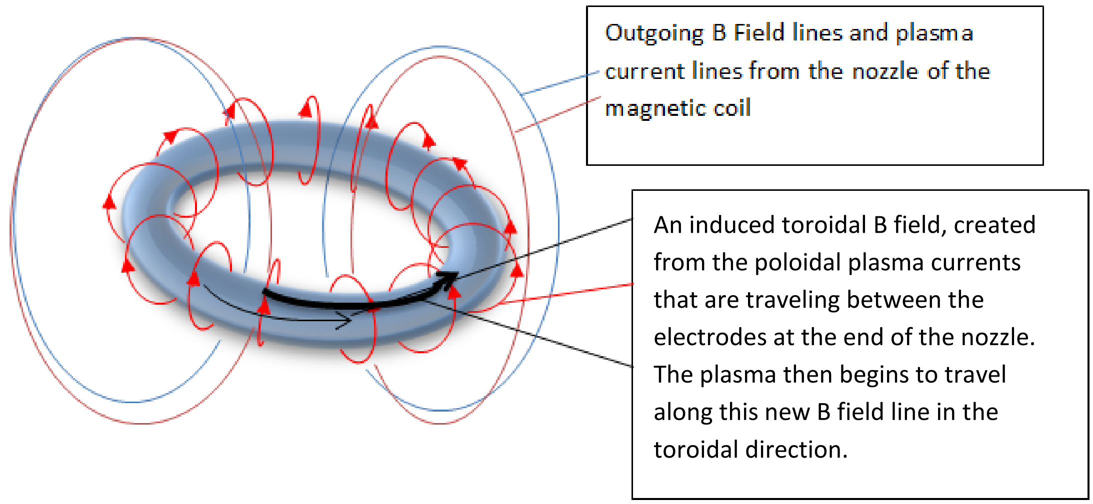

Figure 4: The modified field lines, which show the new B field/plasma current configuration.

Assuming an area across the inner part of the thruster equal to approximately 1.23x 10^{-4}m^2, the poloidal magnetic flux is $\psi_{poloidal} = \boldsymbol{B} \cdot \boldsymbol{A}$ for a given magnetic field, and in this case 0.3 T is used. The alpha parameter varies according to

$$\alpha_{poloidal} = \frac{\mu_0\, I_{poloidal}}{\psi_{poloidal}} \tag{16}$$

, and the relationship between $\alpha_{poloidal}$ and varying inputs of current are given in the chart below, including the default current of 38 A, as was used previously for the thruster without modifications. This gives an $\alpha_{poloidal}$ value of approximately 1.36 m^{-1}.

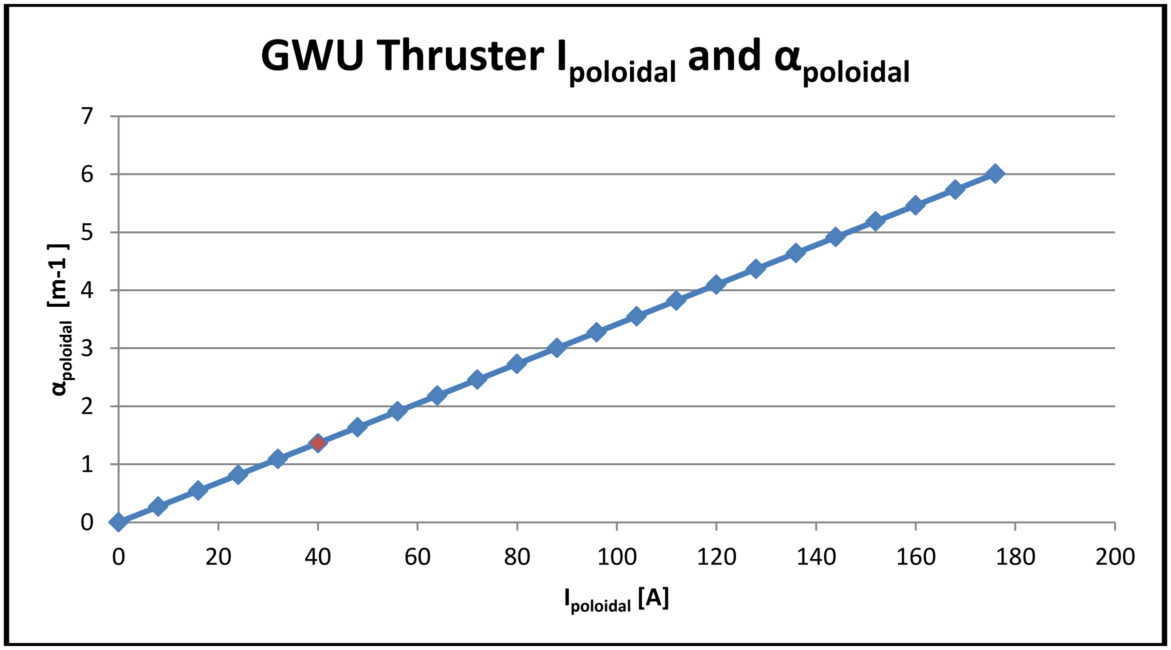

Figure 5: Various values for $\alpha_{poloidal}$, as it pertains to the ability of the GWU μCAT thruster for various currents applied. The red dot is the current value at 38 Amps for experiments conducted during testing.

Kink stability is attainable for the given parameters for the μCAT, according to the Kurskal Stabiltiy Theory [17], which states that an ideal kink instability and column growth can occur, as long as $\alpha_{poloidal}L < 4\pi$, or < 12.57. Therefore, according to the calculated values for $\alpha_{poloidal}$, column lengths of range is not likely to exceed 1 m, and thus the size of the GWU thruster, combined with the required field geometries, could indicate it as a viable candidate for using the collimation method for studying the resistive method of plasma detachment.

The diagnostics and hardware needed to study these characteristics could include spectrum analyzers and tracking generators (spectral) and a charge amplifier or a low noise RF amplifier, to measure image charges from resulting wave density fluctuations [18]. A fast ion gauge would be useful in measuring the density of the spider legs, whose flow velocities are derived utilizing the following equation:

$$\rho\left(\frac{\partial v_z}{\partial t} + v_z\frac{\partial v_z}{\partial z}\right) = \frac{\mu_0 I^2}{2\pi^2 a^3}\frac{\partial a}{\partial z} \tag{17}$$

$$v(z) = \frac{1}{n(z)} \frac{\partial}{\partial t} \int_z^L \frac{\partial n(z')}{\partial t} dz' \quad (18)$$

With ‘a’ being the local flux tube radius, L the length of the plasma filament, I being the total current in the flux tube, v(z) the axial plasma velocity, and n and ρ being the plasma density.

IV. Fusion Spacecraft Propulsion

Fusion propulsion is a means for traveling beyond the Earth to interplanetary, and potentially interstellar space systems. For a full-sized fusion powered spacecraft, loops of copper that generate current will create a magnetic field that guides plasma that is outgoing from the chamber generating the plasma, in the same manner as the magnetic coil of the GWU’s μCAT.

There are various confinement methods available for the production of a fusion reaction for spacecraft, at temperatures greater than 10^8 K and energies in the MeV range. Broadly speaking, these categories are Magnetic Confinement Fusion (MCF) [19], Inertial Confinement Fusion (ICF) [20], Inertial Electrostatic Confinement (IEC) [19], Magneto-Inertial Fusion (MIF), and fission fusion hybrids. There are various factors that play important roles in determining the ideal fuel candidate for the fusion reaction, such as the production of neutrons and neutron capture, the local abundance, and the cost of fuel. Design studies by [22] describe a spacecraft using an MIF propulsion system with an Isp of 19, 436 s and thrust of 3,812 N-sec/pulse. The MIF is achieved with a Z-Pinch annular nozzle, with D-T fuel in the innermost part of the nozzle and Li^6 is in the outermost part of the nozzle. The Lithium is inert and its function is to add mass to the exhaust and to provide an anode return path. Energy is pulsed from capacitors generating 1 GJ, discharging 333 MJ in periods of 100 ns to the DT fuel.

The reactivities can also be used to determine the number of reactions occurring per second for each of these reactions,

$$dN/dt = n_1 n_2 \langle\sigma v\rangle V \ [\#cm^3/sec] \quad (19)$$

with $n_{1,2}$ being the number densities of the fuel #/cm^3, <σv> being the reactivity cm3/sec, and V cm^3 being the volume of the reacting plasma. The value for dN/dt is higher when the D^6Li fuel is a dense solid, and this also helps to make it easier to compress the fuel, compared to a gas. In order to generate fusion for a gas, the density would need to be at a number density of roughly 10^{25} #/m^3, while for a solid it would need to be 10^{29} #/m^3 . Values for the MIF plasma's reactivity rates <σv> are listed in Table 1.

Temp. keV	D-D	D-T	D-^{3}He	T-T	T-^{3}He
10	$1.2x10^{-18}$	$1.1x10^{-16}$	$2.3x10^{-19}$	$7.2x10^{-19}$	$1.2x10^{20}$
100	$4.5x10^{-17}$	$8.5x10^{-16}$	$1.6x10^{-16}$	$1.9x10^{-17}$	$2.7x10^{-17}$
1000	$2.2x10^{-16}$	$2.7x10^{-16}$	$1.8x10^{-16}$	$8.0x10^{-17}$	$5.2x10^{-17}$

Table 1 [23]: For the MIF spacecraft concept, the plasma will range between temperatures of 10 keV to 10^3 keV , with the following reaction rates [cm^3/sec] . This value could be calculated by taking dN/dt and dividing by the number # of reactions.

Out of the various types of nuclear fusion reactions, D^6Li is the only one which has created an output of energy that exceeds its input – specifically demonstrated in thermonuclear bombs. The previous list of reactions provides the elements of the plasma that will be traveling out of the reactor and into the nozzle.

Most of these reactions emit α (^4He) particles, plus some neutrons, Tritium particles, and Hydrogen particles. In some instances, the reactions will produce protons and ^7Be and ^7Li particles. The ^7Be and ^7Li particles are the largest constituents of the plasma in terms of mass, while the α particles are the most numerous.

A. Converting between pulsed and steady plasma flow [2]

The µCAT and most fusion spacecraft utilize pulse plasma propulsion versus steady. The total velocity increment is the sum of increments produced in each pulse Δv, which is equal to

$$\Delta v = v_{e,p} ln \frac{M_0}{M_{lf}} = v_{e,p} ln \frac{M_i}{M_{f,p}} \tag{20}$$

$M_{f,p}$ is the final total mass for the pulse vehicle, $M_i$is the initial total mass of the vehicle, and l_f is the number of pulses needed to produce the velocity increment Δv [2]. For a steady burn,

$$\Delta v = v_{e,s} ln \frac{M_i}{M_{f,p}} \tag{21}$$

Equating the two ratios produces,

$$\frac{M_i}{M_{f,p}} = \left(\frac{M_i}{M_{f,s}}\right)^{\sqrt{\frac{T_s}{T_p}}} \tag{22}$$

With each of the temperatures being the temperature in the reservoir for the steady state and pulsed spacecraft, and the burn time dilation factor being represented as $\sqrt{\frac{T_p}{T_s}}$. The hypothesized high temperature of the pulsed plasma will give an efficient utilization of fuel mass in comparison to the steady burn. Pulsed plasma generation also gives a more efficient coupling of plasma to the B field. The operational burn times can thus be calculated, as

$$\frac{(\Delta t)_p}{(\Delta t)_s} = \left(\frac{M_{i,p}}{M_{i,s}}\right)\left(\frac{T_p}{T_s}\right)\frac{1-\left(\frac{M_{f,s}}{M_{i,s}}\right)^{\sqrt{\frac{T_s}{T_p}}}}{1-\frac{M_{f,s}}{M_{i,s}}} \tag{23}$$

Which indicated that the operational burn time is longer for a pulsed spacecraft than for the steady burn, and therefore, the on-board energy storage would need to be increased by a factor equal to the time dilation factor in order to achieve a given velocity increment.

B. Scaling up

In order to accurately utilize small pulsed-plasma thrusters in modeling full-scale fusion spacecraft, mathematical relationships for plasma scaling will need to be employed. The principals of plasma laboratory modeling indicate that: firstly, there is an equality of velocities and energies for both small and large spacecraft, and once the characteristic scaling factor γ is obtained one may: secondly, relate other attributes of plasma phenomenon. This can be done using the linear properties of Maxwell's equations and equations of motion, with the velocity and the electron temperature to stay the same (in eV), magnetic fields altered by a factor of γ, and density is influenced by a factor of γ^2.

The scaling factor γ is obtained by estimating the length ratio between the laboratory sized nozzle and the full sized nozzle. The nozzle for the thruster used in the laboratory setting is on the scale of approximately 10^{-2}m while the size of the nozzle used on the fusion spacecraft is on the scale of between 10^{1}m to 10^{0} m. Therefore, a value of 150 would be appropriate for γ for scaling up or down the plasma parameters when conducting nozzle experiments.

V. Conclusions

This method of resistive detachment could work for magnetic nozzles being utilized in pulsed-plasma (and potentially steady plasma) spacecraft, given that we are able to generate the same mechanism of toroidal B field and plasma current flow and spheromak formation as in the collimation experiments modeling solar plasma activity. The future experiments with the µCAT could be conducted with an inner copper cathode, most likely constructed from a piece of pipe, from which multiple sparks are generated, to greet plasma being generated on the outer annulus electrode ring located on the outside of the magnetic coil of the thruster nozzle. It may be interesting to explore further that other types of instabilities are present – such as helical and kink, with the onset of helical instability being driven by the Kruskal-Shafranov condition, as shown by experiment [1].

VI. References

[1] Hsu, S.C. Bellan, P.M. A Laboratory Plasma Experiment for Studying Magnetic Dynamics of Accretion Dics and Jets. Mon. Not. R. Astron. Soc. 334, No. 2, 257-261 (2008).

[2] Gerwin, R.A., Marklin, G.J., Sgro, A.G., Glasser, A.H. Characterization of Plasma Flow through Magnetic Nozzles. AL-TR-89-092. DTIC report Feb (1990).

[3] Sankaran, K. and Polzin, K. Development of Numerical Tools for the Investigation of Plasma Deatchment from Magnetic Nozzles, 38th AIAA Plasma Dynamics and Lasers Conference, Miami, FL. June 25-28, (2007).

[4] Arefiev, A.V., Breizman, B.N. Magnetohydrodynamic Scenario of Plasma Detachment in a Magnetic Nozzle. Physics of Plasmas 12, 043504 (2005).

[5] K. Sankaran and K. Polzin, Numerical Investigation of Near-Field Plasma Flows in Magnetic Nozzles, *45th AIAA/ASME/ASEE/SAE Joint Propulsion Conference*, Denver, CO, Aug. (2009).

[6] Ahedo, E. Plasma Dynamics in a Helicon Thruster, Progress in Propulsion Physics 4, 337-354 (2013).

[7] Ahedo, E and Merino, M. On Plasma Detachment in Propulsive Magnetic Nozzle, Physics of Plasmas 18, 053504 (2011).

[8] Lapenta, G Knoll, D. A.. Reconnection in the Solar Corona: Role fo the Kelvin-Helmholtz Instability Solar Physics 214: 107 – 129, (2003).

[9] Brackbill, J.U. and Knoll, D. A. Transient Magnetic Reconnection and Unstable Shear Layers, Physical Review Letters, Vol 86, 11, 2329-2332 (2001).

[10] Brackbill, J.U. FLIP MHD: A Particle-in-Cell Method for Magnetohydrodynamics, Journal of Computational Physics Vol 96, 163-192 (1991).

[11] Lapenta, G. and Knoll, D. A.: Effect of a Converging Flow at the Streamer Cusp on the Genesis of the Slow Solar Wind, Astrophysics Journal, 624, 1049–1056, doi:10.1086/429262, (2005).

[12] Elskens Y., Escande, D. Microscopic Dynamics of Plasmas and Chaos. Institute of Physics Publishing (2003).

[13] Matthaeus, W.H. et al. Fluid and kinetic structure of magnetic merging int eh Swarthmore Spheromak Experiment. Geophysical Research Letters, Vol 32, L23104 (2005).

[14] Brown, M.R. et al. Energetic particles from three dimensional magnetic reconnection events in the Swarthmore Spheromak Experiment, Physics of Plasmas, Vol 9 No. 5, (2002).

[15] You, S., Yun, G.S., Bellan, P.M. Dynamic and Stagnating Plasma Flow Leading to Magnetic Flux Tube Collimation. Physical Review Letters 95, 04500 (2005).

[16] Zhuang, T. et al, Ion Velocities in a Micro-Cathode Arc Thruster, Physics of Plasmas 19, 063501 (2012).

[17] Bateman G., MHD Instabilities. MIT Press, Cambridge, MA, (1978).

[18] Danielson, J.R. Measurement of Landau Damping of Electron Plasma Waves in the Linear and Trapped Regions. University of California San Diego, PhD dissertation http://sdphca.ucsd.edu/pdf_files/danielson_thesis.pdf

[19] Bussard, R.W. Fusion as Electric Propulsion. Journal of Propulsion, 6:5, 567-574 Sept-Oct (1990).

[20] Orth, C.D. VISTA – A Vehicle for Interplanetary Space Transport Application Powered by Inertial Confinement Fusion. Lawrence Livermore Laboratory National Laboratory technical document, UCRL-TR-110500.

[21] Nebel, R. A. et al. Theoretical and Experimental Studies of Kinetic Equilibrium and Stability of the Virtual Cathode in an Electron Injected Inertial Electrostatic Confinement Device. Physics of Plasmas, 12:1, (2005).

[22]Miernik, et al. Z-Pinch Magneto-Inertial Fusion Propulsion Engine Design Concept. Seventh IAA Symposium on Realistic Near-Term Advanced Scientific Space Missions. Aosta, Italy, July 11-14, (2011).

[23] Huba, J.D. NRL Plasma Formulary. p. 43